RESULTS FROM FIRST SPACE DEBRIS SURVEY OBSERVATIONS IN MEO

European Space Surveillance Conference
7-9 June 2011

A. Hinze[1], T. Schildknecht[1], A. Vananti[1], H. Krag[2]

[1] *Astronomical Institute, University of Bern,*
Sidlerstrasse 5, CH-3012 Bern, Switzerland,
andreas.hinze@aiub.unibe.ch, thomas.schildknecht@aiub.unibe.ch, alessandro.vananti@aiub.unibe.ch

[2] ESA/ESOC,
Robert-Bosch-Strasse 5, D-64293 Darmstadt, Germany,
holger.krag@esa.int

ABSTRACT

The Medium Earth Orbit (MEO) region becomes increasingly populated as new navigation satellite constellations are deployed or existing constellations are replenished with new satellites. As a consequence a growing number of space debris including small-size objects can be expected. Based on the findings for the GEO region one could expect small-size operational debris, delamination debris from aging objects, and debris from fragmentation events. The Astronomical Institute of the University Bern (AIUB) performed several survey campaigns between January 2010 and November 2010 to search for debris objects in the MEO region. The optical observations were conducted in the framework of an ESA study using ESA's Zeiss 1-m telescope located at the Teide Observatory at Tenerife, Spain. To estimate the population and the density of debris objects in MEO orbits, first surveys covering particular orbital planes of the GLONASS and GPS constellations have been performed. These orbital planes include a high number of operational and defunct satellites, as well as spent upper stages. The results from the different observation campaigns will be presented. Based on the measured data a statistical analysis was performed to estimate upper limits for the debris density in the investigated orbital planes.

INTRODUCTION

The largest part of the mass launched into space actually becomes 'space debris' or 'orbital debris' immediately after launch. After the accomplished mission even the payload will become space debris eventually. The increasing number of space debris creates an increasing risk for man-made missions. In higher regions where no "natural" clean-up effects exist the only way of dealing with the space debris threat is the continuous observation of the space debris environment. While the low Earth orbits (LEO) have been extensively studied during the last decades and the geostationary ring (also called geostationary Earth orbit, GEO) and the geostationary transfer orbits (GTOs) have been continuously observed during the last years the next logical step is the extension of the ongoing space debris surveys to new orbital regions, in particular to the increasingly populated medium Earth orbit (MEO) region. The space debris environment in the MEO region has not been systematically investigated so far and is thus largely unknown.

EXPLOSION MODEL AND SIMULATED POPULATION

At first a reference population based on the DISCOS catalogue of June 2009 was generated. A refined MEO definition was used, focusing on the objects with a mean motion between 1.5 and 2.5 revolutions per day. A second filter selected an eccentricity smaller than 0.2. The results comprise 214 objects, including 50 GPS satellites and 109 GLONASS satellites.

In order to identify possible debris clouds due to explosions in the MEO region, a set of fragmentations has been simulated, taking into account a reasonable range of ejection velocities as a function of the fragment size. For the breakup model we have referred to the study of Pardini and Anselmo [1]. Assuming debris of spherical shape the cumulative number of fragments as a function of the diameter can be calculated (Figure 1 left). In the explosion model an isotropic ejection of the fragments was assumed and their distribution of the velocity is shown in Figure 1 right.
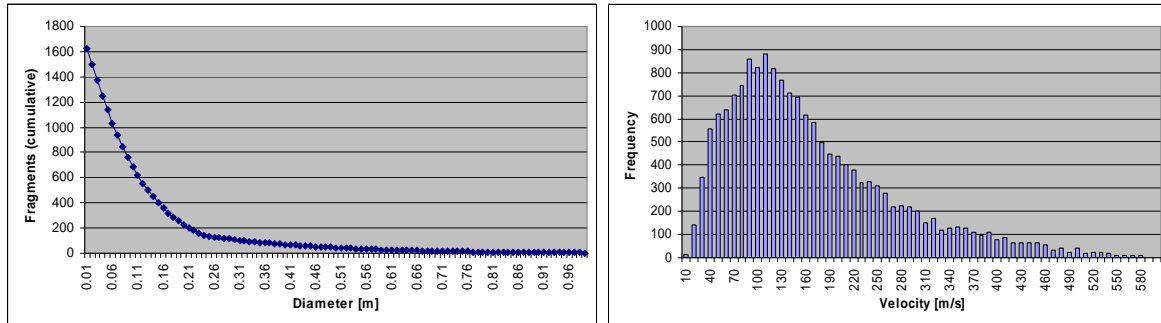
Figure 1. Cumulative number of fragments as a function of the diameter (left) and the distribution of the velocity of the fragments (right).

The culmination point and the ascending node were selected as representative locations along the orbit for the explosion. The choice of the location is relevant when the orbit is analyzed through its orbital elements. Due to the explosion the orbit of the fragments will differ from the original orbit. Depending on the plane orientation change, either the right ascension of the ascending node (RAAN) or the inclination will show a larger variation. GPS and GLONASS orbits were taken into account and the distributions of the single orbital elements after the explosions were calculated. As a consequence of the explosion the distribution of the semi-major axis is broadened around the value of the original orbit with a deviation of about 1000 km. All the fragments show a more excentric orbit than the one of the parent object, with a broad range of values between 0.01 and 0.1 and a highest value of 0.03. The analysis of the inclination and the RAAN showed that the fragmentation at the node is characterized by a narrow dispersion in the RAAN and a wide spreading in the inclination. If the breakup event happens at the culmination point the situation in RAAN and inclination is right the opposite. Furthermore the argument of perigee and, after few complete orbits, the mean anomaly, are homogeneously distributed.

Since a fragmentation event can occur to each of the MEO objects in the reference catalogue, the next step consists in applying the explosion dispersion to the distribution of the reference population. The convolution of the two distributions was calculated for all orbital elements. In the excentricity the dispersion due to the explosion is predominant, whereas in the ascending node the width is mostly characterized by the existing population distribution. The convoluted elements values have an approximate Gauss distribution. Finally the evolution over time of the orbital elements was considered. We referred to the "Detailed assessment of a European Space Surveillance System" study [2]. In this study orbit propagations over many years were done using the following forces: lunisolar perturbations, Earth's potential up to degree and order 30, Earth tides, general relativity and the direct radiation pressure. JPL DE200 ephemeris data for Moon and Sun, the JGM3 model for the Earth potential, and the UTCSR ocean tide model were used. Taking the age of the satellites into account the explosion distribution was convoluted with the deviations in the orbital elements after 15 years. Assuming that the deviations can be described with a Gauss distribution, the resulting distribution can be characterized by a standard deviation, composed by the explosion and evolution deviations: $\sigma^2_{tot} = \sigma^2_{expl} + \sigma^2_{evol}$.

Table 1. Summary of the deviations in the orbital elements

Description	σ expl.	σ evol.	σ tot.
A [km]	1200	~ 0	1220
e	0.02	0.01	0.022
i [°]	1.5	0.5	1.6
RAAN [°]	5	5	7

A synthetic population of 1000 objects was generated using Gaussian distributions with the total deviations and with the centers at the average orbital elements of different subgroups in the reference population. Figure 2 shows the poles of the orbit planes of the population in a gnomonic representation. A given observation field with a right ascension α and a

declination δ is crossed by all orbits with inclinations i equal to or larger than $|\delta|$ and ascending node Ω that fulfill the equation:

$$\sin(\alpha - \Omega) = \tan(\delta)\cot(i).$$

(1)

In the (Ω, i) space the latter equation defines a stripe of finite width depending on the FOV of the optical sensor. In this representation the stripes are delimited by straight parallel lines. The covered field is identified with the normal to the stripe through the center of the diagram. The azimuth of the normal line and the radius, from the center up to the stripe, are directly related to the (α, δ) field.
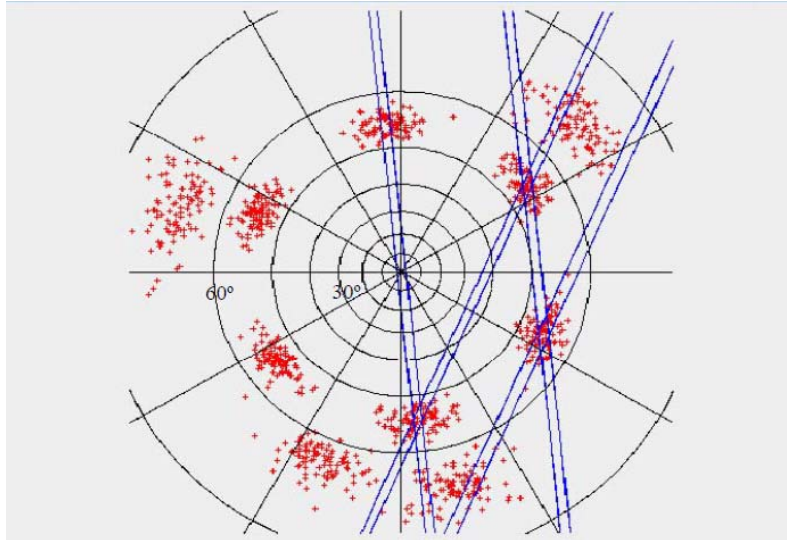
Figure 2. Poles of orbit planes of the synthetic population (gnomonic projection)

SURVEYS

For the MEO surveys we assumed interesting concentrations of unknown objects in the orbit regions around GPS and GLONASS satellites constellations. It is possible to divide these satellite constellations in six groups of GPS satellites and three groups of GLONASS satellites. Each group represents a set of several orbits approximately lying on the same orbit plane. Figure 3 shows geocentric orbit plots of all known catalogue objects in GLONASS and GPS planes. Orbits in red colour are active satellites whereas black indicates non-active satellites. Depending on the season and of the preferred observation geometry not all such orbit planes were observable from the ESA Space Debris Telescope (ESASDT) during this time.
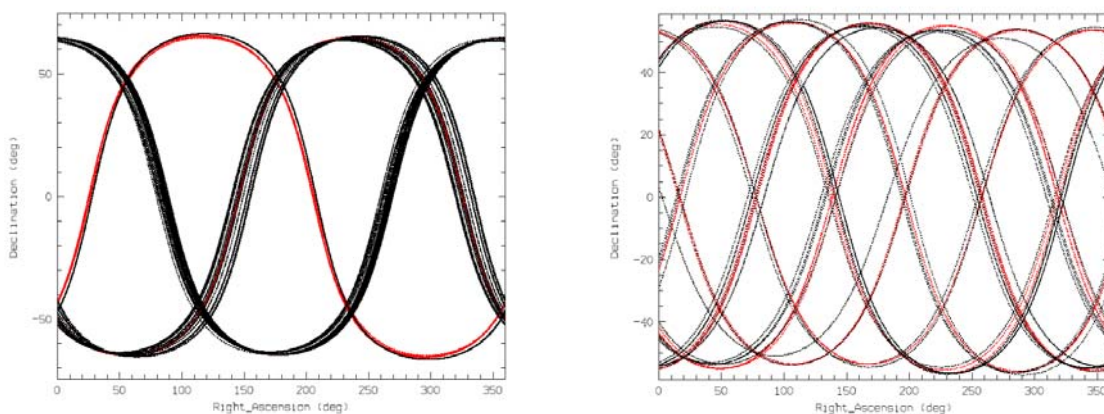
Figure 3. Plot of the geocentric orbits of all GLONASS (left) and GPS (right) satellites. Active satellites are in red colour and non-active satellites in black.

During the time between January 2010 and November 2010 on 44 nights 284 surveys were performed. This corresponds to 3124 minutes (≈ 52 hours) of observations. Here one survey is to understand as the observation of one field during 11 minutes, the time needed for the acquisition of 29 frames. A summary for all campaigns is shown in Table 2 with the number of surveys per satellite group. The last row includes the total observation time.

Table 2. Number of surveys given for each satellite group. The last row gives the total observation time.

Group/Plane	N1	N2	N3	N4	N5	N6	G1	G2	G3
January	14	0	0	6	0	0	8	0	0
February	8	0	0	8	0	0	0	0	0
March	2	0	0	3	0	0	14	8	0
April	0	5	0	0	0	0	6	5	0
May	0	0	0	0	0	0	0	37	0
June	0	0	0	0	0	0	0	0	0
July	0	0	0	0	0	0	0	0	0
August	0	0	0	0	0	0	0	0	0
September	1	0	0	0	0	0	3	15	0
October	0	0	14	0	0	0	33	3	0
November	0	0	0	0	0	0	0	0	91
Time in min.	275	187	55	154	0	0	704	748	1001

Because of the assumption of more objects in GLONASS planes than in GPS planes almost all surveys after February have been performed in GLONASS orbit planes. Towards the end of the year other orbit planes were visible and for a statistical analysis some surveys were performed again in the GPS planes.

In Table 3 all nine groups of satellites with their approximate RAAN (January 2010) are shown. In the second and third raw the number of active and non-active satellites is given. Some orbit planes of GPS and GLONASS satellites have the same RAAN but they differ in the inclination. A typical inclination of GPS satellites is around 55° while GLONASS satellites have a typical inclination of about 65°.

Table 3. Groups of GLONASS and GPS satellites.

	GLONASS			GPS					
Group/plane	G1	G2	G3	N1	N2	N3	N4	N5	N6
RAAN	30	150	270	30	150	210	90	270	330
active	8	8	5	5	5	5	6	6	4
non-active	9	42	44	2	4	1	3	3	4

Based on exact orbits of some visible satellites the coordinates for each field have been determined. This includes right ascension of the ascending node, declination as well as the expected range and the assumed speed.

ANALYSIS AND RESULTS

During the MEO survey campaigns no new object was found. Nevertheless, from the observed fields and the survey duration per field, and assuming the previously considered explosion population it is possible to hazard statistical considerations about the real debris population in the MEO region. The observed fields in RA / DE correlate to regions in the inclination / RAAN space as described in Figure 2. These regions in turn determine the number of objects of the hypothetical population that can be detected. The number is related to the volume defined by the section of the two-dimensional normal distribution of the population delimited by the FOV of the telescope. The integral of the cross section is easiest to calculate when the measurements are done at the point of maximal declination (culmination) or at the orbital node of the observed orbit, e.g. for GPS satellites the culmination would be around 55 deg declination. In this case the calculation reduces to a one-dimensional integration over the interval delimited by the FOV.

Figure 4 is an example of the coverage performed during the survey campaigns for one GLONASS orbital plane. The diagram wants to give an idea of the coverage in terms of number of fields observed, but it does not show the real observed coordinates. Only the coordinates of the middle of the stripe indicate approximately the DE / RA of the actually observed field. The length of the stripes denotes the total observation time of the single field expressed in number of equivalent fields. With the assumption of a 70 s dwell time, a 10 minutes survey on one field, since the objects have moved in the mean time, correspond to the equivalent of 8.5 fields, a stripe length of 8.5 x 0.7 deg ≈ 6 deg. During the survey campaign the same field was repeatedly observed at different times and on several nights. Therefore the indicated stripes in general have arcs longer than 6 deg. The position of the stripe with respect to the nominal orbit (blue dotted line with culmination at 64.5 deg for GLONASS) shows that orbital planes with inclinations different than the nominal inclination were observed in the culmination.
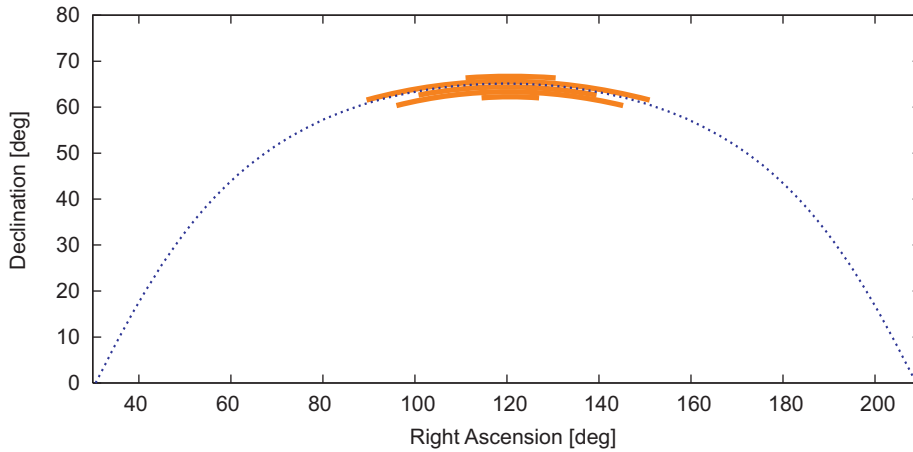
Figure 4. Simplified representation of the number of observed fields in the survey of the group G1.

Since the surveys do not cover the observed fields for the entire revolution period of an object it is only possible to make some statistical considerations. As an example for the culmination surveys the number of observed fields per inclination is shown in the above diagram for the group G1. On the other hand the total number of observable fields in one inclination stripe is 360 deg / 0.7 deg = 514. For the rest of the document the latter will be simply called "fields", whereas the fields really pointed by the telescope during the surveys will be called "RA/DE fields". The statistical problem is similar to the classical distribution of k successes in a sequence of n independent yes/no experiments, each of which yields success with probability p. In statistics the problem is described by the binomial distribution:

$$p_k = \binom{n}{k} p^k (1-p)^{n-k}$$

(2)

Applied to our surveys, k = 0, since no new object was found, n is the number of observed fields, and p is the searched probability. Here we assume that the choice of the survey fields is casual, which corresponds more or less to reality because the time of observation during the night varied considerably and was arbitrarily decided by the observer at ESASDT. Furthermore in the following considerations we assume that at most one object per field can be found. The assumption is justified by the fact that k is very small compared to n, consequently also p will be quite small and the probability of two objects on the same field is almost vanishing.

The common estimator p' for the binomial distribution yields p' = k/n = 0. More useful is to determine a confidence interval [p_l, p_u] with a lower limit p_l and an upper limit p_u around p'. For a 95% confidence level with k = 0, the lower limit is p_l = 0, while p_u is determined according to the area of the distribution delimited by k.

When k and n are given, and p is the unknown, it is comfortable to use one of the existing statistics tools for the calculation, e.g. the "betainv" function in the Excel software. The unknown p_u, for a 95% confidence level with k = 0, is calculated with:

$$p_u = \beta^{-1}(95\%, 1, n) .$$

(3)

In the following tables the total number of fields is given by a normalized sum over the fields at different inclinations/nodes. For the surveys in the culmination the normalization factor is simply the integral under the normalized population distribution at the given inclination, delimited by the FOV.

Table 4, Table 5 and Table 6 summarize for the groups N1, N2, and N3, the number of observed fields and the estimated upper limit, according to p_u, of number of objects present in the group. The number of samples (fields) for the GPS survey is not very high and the estimated limit is consequently quite large.

Table 4. Number of fields/objects for the N1 group.

# Fields	Incl. [deg]	Norm.	Norm. # fields
180	53.6	0.12	21
# Objects			73

Table 5. Number of fields/objects for the N2 group.

# Fields	Incl. [deg]	Norm.	Norm. # fields
43	53.6	0.12	5
# Objects			308

Table 6. Number of fields/objects for the N3 group.

# Fields	Incl. [deg]	Norm.	Norm. # fields
42	54.3	0.16	7
26	53.6	0.12	3
34	52.2	0.04	1
Sum			11
# Objects			140

The number of observed fields and estimated objects for the groups G1, G2, and G3 is given in Table 7, Table 8 and Table 9. In general for the GLONASS surveys there is a better statistics than for the GPS case and the inferred limits for the objects number indicate more reasonable values. For the G3 group the RA/DE fields were not chosen close to the orbit culmination because of visibility constraints. Table 9 indicates for every RA/DE field the according RAAN/Inclination of the orbit closest to the nominal GLONASS orbit among the orbits covered by the field. In fact one RA/DE field includes a range of inclinations and nodes. While a field in the culmination includes the whole node range of the population, an arbitrary one covers only a reduced region in the inclination/node space. The direct way to determine the inclination/node range is to evaluate the volume integral of the cross section of the two-dimensional normalized population distribution. In a representation of the two-dimensional Gauss distribution in a xyz reference system, the section would be delimited by two parallel planes parallel to the z axis (Figure 5), while their orientation is related to α and Ω. The calculated integral corresponds to the normalization factor. The upper limit for the G3 group is a surprisingly small number of 6 objects.
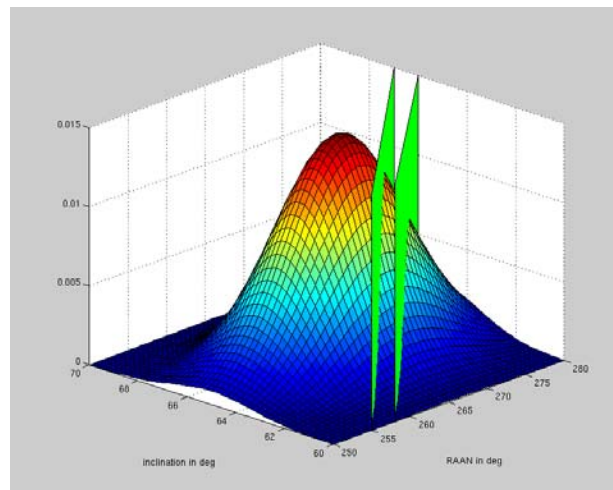
Figure 5. Plot of the Gauss distribution of the inclination and RAAN of G3.

Table 7. Number of fields/objects for the G1 group.

# Fields	Incl. [deg]	Norm.	Norm. # fields
17	62.4	0.07	1
77	63.1	0.12	9
60	63.8	0.16	9
94	64.5	0.17	16
34	65.2	0.16	5
Sum			40
# Objects			38

Table 8. Number of fields/objects for the G2 group.

# Fields	Incl. [deg]	Norm.	Norm. # fields
377	64.5	0.17	65
94	63.1	0.12	11
Sum			76
# Objects			20

Table 9. Number of fields/objects for the G3 group.

# Fields	RA [deg]	DE [deg]	RAAN [°]	Incl. [deg]	Norm.	Norm. # fields
26	270.5	6.92	266.6	64.5	0.18	5
60	290.5	40.1	266.6	64.5	0.24	15
77	307.0	53.63	266.6	64.5	0.35	27
68	283.5	30.63	266.6	64.4	0.21	14
188	293.5	43.2	266.6	64.4	0.26	49
137	83.25	7.08	266.6	64.5	0.17	24
120	311.75	55.58	266.6	64.4	0.39	47
51	315.0	57.87	266.6	64.4	0.42	22
51	78.5	17.25	266.6	64.4	0.18	9
103	301.75	50.08	266.6	64.4	0.32	33
Sum						244
# Objects						6

If we recall the fragment distribution (Figure 1) in the explosion model discussed previously, we can expect around 200 objects with a limiting size for the ESASDT of 20 cm. This might lead with some precaution to the statement that no explosion has occurred at least in the examined GLONASS orbits. On the other hand, the model is based on assumptions, treated previously, on the explosion process and on the propagation of the debris fragments, thus it might not thoroughly reflect the real conditions.

CONCLUSIONS

The highest probability of space debris created by an explosion in the MEO region is in the orbit planes of GPS and GLONASS satellites constellations. Surveys have been performed in all GLONASS planes and in three of the GPS planes. Based on these surveys, where no new object was found, an upper limit for the debris population in the observed satellite groups could be determined. In the GLONASS orbits the limit does not exceed the value expected from an explosion which leads to believe that no explosion has actually occurred. These results are based on a quite limited number of observed regions and more investigations should be done to estimate the real debris population density in MEO.

REFERENCES

[1] Pardini, C., L. Anselmo, 'Dynamical evolution of debris clouds in geosynchronous orbit', Advances in Space Research 35, pp. 1303-1312, 2005

[2] Donath, Th., T. Schildknecht, P. Brousse, J. Laycock, T. Michal, P. Ameline, L. Leushacke, 'Detailed Assessment of a European Space Surveillance System', Final Report ESA/ESOC Contract 18574/04/D/HK(SC), 2005.